Modeling Kinetic Shifts and Competition in Threshold Collision-Induced Dissociation. Case Study: *n*-Butylbenzene Cation Dissociation

Felician Muntean[†] and P. B. Armentrout*

Department of Chemistry, University of Utah, Salt Lake City, Utah 84112

Received: May 8, 2003

A threshold collision-induced dissociation (TCID) study was performed on the *n*-butylbenzene cation, investigating the competitive dissociation leading to propyl and propene elimination. Ab initio calculations at the B3LYP/6-311++G(2d,2p)//B3LYP/6-31G* level were performed on the system. Reaction path calculations were performed for both dissociation channels to provide details of the dissociation mechanisms and to identify rate-determining transition states. Unimolecular dissociation rates as a function of energy from literature PEPICO and PD-MIKES experiments are modeled using RRKM statistical unimolecular decay theory to select the best calculated transition states for the two dissociation channels. The effects of kinetic and competitive shifts on the CID threshold determinations are investigated and explained using a model that incorporates RRKM theory. Final analysis of the TCID data yields 0 K dissociation energies of 1.70 ± 0.09 eV for the propyl elimination channel and 1.28 ± 0.06 eV for the propene elimination channel. On the basis of the current and previous studies, we identify procedures for selecting appropriate transition states when the feedback obtained from experimental dissociation rates is not available.

Introduction

This paper is part of a series of studies designed to improve the accuracy of thermochemical measurements by threshold collision-induced dissociation (TCID).[1−9] The series was designed to test the validity of the procedures used in modeling TCID data, especially with regard to the treatment of kinetic and competitive shifts.[10−14] As recently described,[15,16] the concept is to perform CID on a system for which both the energetics and the unimolecular dissociation rates as a function of energy are experimentally known. For such a system, uncertainties related to the ambiguity of transition state (TS) location and to the Rice−Ramsperger−Kassel−Marcus (RRKM) calculation[17] of unimolecular dissociation rates are largely eliminated. The system should also dissociate slowly enough to yield observable kinetic shifts on our instrument (slower than $1-5 \times 10^{-4}$ s). By using the experimental dissociation rates in our analysis and by comparing CID thresholds with the known energetics, we can obtain feedback on improving our model.

Two previous studies in this series investigated systems chosen as prototypes for two very different cases of molecular dissociation. The first case is a simple bond breaking, the CID of the *ortho*- and *para*-dichlorobenzene molecular cations[15] leading to atomic Cl loss. The second case is a multiple-step, complex rearrangement dissociation, the CID of the phenol cation leading to CO loss.[16] Both studies indicated that selecting the correct transition state is important for obtaining reliable thermochemistry from CID data of relatively large molecular systems and that detailed quantum chemical calculations are a useful tool. In the case of Cl loss from dichlorobenzene cations, where a loose transition state might be expected for the simple bond cleavage, the study revealed that a moderately tight transition state was more appropriate. We concluded that a phase-space limit (PSL) or orbiting transition state does not properly characterize the breaking of a covalent chemical bond as in this system. In the second case, the loss of CO from phenol cation, the study indicated that kinetic shifts are correctly taken into account by our CID model when the rate-determining, tight transition state is clearly identified by ab initio calculations.

In the present paper, we investigate the lowest-energy dissociation channels of the *n*-butylbenzene cation, reactions 1 and 2. This molecular system includes both types of dissociation that we investigated in the previous studies described above: a simple bond cleavage, reaction 1, and dissociation through complex rearrangement, reaction 2. In addition, this system exhibits a strong competition between the two channels, an additional element of complexity to be considered in CID data modeling.

$$n\text{-}C_4H_9C_6H_5^+ \rightarrow C_7H_7^+ + n\text{-}C_3H_7 \quad (1)$$

$$\rightarrow C_7H_8^+ + C_3H_6 \quad (2)$$

The branching ratio between the two products above has been found to be a sensitive measure of the internal energy content of the molecule, suggesting the use of the system as a molecular thermometer. For this reason, this dissociation has been extensively investigated for over two decades through a variety of techniques.[18−29] The key factor was to correctly measure the internal energy deposited in the molecule. One of the most detailed and reliable investigations is that of Baer et al.,[27] who used photoelectron−photoion coincidence (PEPICO) to determine dissociation rates and branching ratios of the two products as a function of photon energy. The dissociation rates for reaction 2 were determined in the range between 10^5 and 10^6 s^{-1}. The previous photodissociation ion cyclotron resonance (PD-ICR) study of Chen et al.[22] provided several additional reaction rates in the same range. More recently, the photodissociation mass-analyzed kinetic energy spectrometry (PD-

* To whom correspondence should be addressed. E-mail: armentrout@chem.utah.edu.

[†] Current address: JILA, University of Colorado, Boulder, CO 80309.

10.1021/jp035256g CCC: $25.00
Published on Web 08/20/2003

TABLE 1: Literature Thermochemistry for *n*-Butylbenzene Ion Dissociation[a]

species	$\Delta_f H°_{298}$ (neutral, kJ/mol)	$\Delta_f H°_0$[b] (neutral, kJ/mol)	IE (eV)	$\Delta_f H°_0$[c] (ion, kJ/mol)
n-$C_4H_9C_6H_5$	−13.1 (1.1)[d]	26.4 (1.1)	8.69 (0.01)	864.8 (1.5)
C_7H_7	207 (4)	226.5 (4)	7.242 (0.006)	925.2 (4.0)
n-C_3H_7	96.6 (3.4)[e]	113.7 (3.4)		
C_7H_8[f]	150 (10)	172.4 (10)	8.0 (0.1)	944.3 (13.9)
C_3H_6	20.0 (0.8)[d]	35.0 (0.8)		

[a] From ref 32 unless otherwise specified. Enthalpies of formation expressed in the ion convention. Uncertainties in parentheses. [b] Converted to 0 K using the calculated vibrational frequencies from Table 3. [c] Calculated using the neutral values and the ionization energies. [d] Reference 34. [e] Reference 33. [f] Methylene-1,3-cyclohexadiene.

MIKES) studies of Oh et al.[28] contributed several other rates in the 10^8 s^{-1} range, which considerably improves the accuracy of the modeling of dissociation rates through RRKM.

The current understanding of the dissociation mechanism of *n*-butylbenzene can be summarized as follows. Reaction channel 1 leads to the benzyl ion (91 amu) and the *n*-propyl neutral, a simple bond cleavage dissociation.[22,27] This pathway has a higher energy onset than reaction channel 2, which leads to the methylene-1,3-cyclohexadiene ion (92 amu) and the propene neutral.[27,30] This path has no measurable reverse activation barrier[31] in excess of the reaction endothermicity, but because of the molecular rearrangement required, it is believed to involve an intermediate complex formation and a tight TS.[27]

The thermochemistry of this system is reasonably known for both the reactants and the products. Relevant literature values[32−34] are presented in Table 1 and indicate that, at 0 K, reaction 1 is endothermic by 174.1 ± 5.2 kJ/mol (1.80 ± 0.05 eV) and reaction 2 is endothermic by 114 ± 14 kJ/mol (1.19 ± 0.14 eV). (Somewhat different values are listed by Baer et al.[27] largely because they used an older value for the heat of formation of the propyl radical.) The dissociation thresholds for the two reactions have been measured by a variety of techniques. Among these, PEPICO[27] and PD-MIKES[28] provided values that account for kinetic shifts, although the accuracy of these values depends strongly on a correct estimation of the molecular parameters in the RRKM calculation of the dissociation kinetics, a problem discussed in detail below.

The present work describes a threshold CID study of the *n*-butylbenzene cation dissociation, reactions 1 and 2. Detailed quantum chemical calculations were also performed on the system to complement the available information about the dissociation mechanisms and to provide the necessary molecular parameters needed for the analysis of the experimental data. Dissociation rates for the 91 and 92 amu channels obtained in the PEPICO[27] and PD-MIKES[28] experiments are modeled using RRKM theory, to investigate the most probable transition state assumptions for this dissociation. The appropriate transition states are then used in modeling the CID cross sections to account for kinetic shifts and competition. The dissociation thresholds obtained are compared to the literature values and to theoretical results.

Experimental and Data Analysis

Instrumentation. The guided ion beam tandem mass spectrometer instrument used in this study has been previously presented in detail.[14,35] Briefly, the instrument comprises an ion source, a mass selector, a reaction region surrounding an octopole ion guide, a second mass selector, and a detector. The ion source used here is a microwave discharge, followed by a 1-m-long flow tube, with He as a buffer gas at pressures ranging from 0.5 to 0.8 Torr. Vapors of *n*-butylbenzene are introduced into the flow tube ion source through the inlet port located about 0.5 m from the microwave discharge. The *n*-butylbenzene cations are formed by collisions with He ions and metastables and thermalized by many collisions ($>10^5$) with He in the flow. Sample ions drift out of the flow tube and are focused through two regions of differential pumping, accelerated, focused into a magnetic field for mass selection, decelerated using an exponential retarder, and focused into the octopole ion guide region.

The TCID experiments were performed on both the current double-octopole configuration of our instrument[14] and the previous single-octopole configuration,[35] yielding comparable results. The reaction cell is placed around the first octopole, and CID with Xe takes place here. The energy spread of the reactant ion beam in this region is about 0.25 eV fwhm, as measured by retarding potential analysis, which also ascertains the absolute zero of the reactant ion kinetic energy within about 0.05 eV. Typical Xe pressures in the cell vary between 0.05 and 0.2 mTorr. Product and unreacted primary ions drift to the end of the octopoles; are focused into the second mass selector, a quadrupole mass filter; and then are detected by a Daly-type detector.[36] The method of measuring absolute integral cross sections on this instrument has been previously described in detail.[35] Briefly, intensities for reactant and all product ions are measured as a function of the interaction energy and target gas pressure in the collision cell and then converted to cross sections. Energies are converted from the laboratory frame of reference to the center-of-mass frame using $E_{CM} = E_{lab}M/(M + m)$, where M is the mass of the neutral reactant and m is the mass of the reactant ion.

Data Analysis. Thermodynamic information provided by the low-energy TCID experiments is extracted from the energy dependence of the integral cross sections in the threshold region. In cases in which two or more product channels are in competition with one another, the formation of higher-energy products can be inhibited, such that their detection might be possible only at energies that are higher than the actual thresholds. This leads to what are usually called competitive shifts. To account for such competition, we use the model derived and discussed in a previous paper.[13] Briefly, the equation used is

$$\sigma_j(E) = \frac{n\sigma_{0,j}}{E}\sum_i g_i \int_{E_0-E_i}^{E} \frac{k_j(\epsilon + E_i)}{k_{tot}(\epsilon + E_i)} \times [1 - e^{-k_{tot}(\epsilon+E_i)\tau}](E - \epsilon)^{n-1}\, d\epsilon \quad (3)$$

where σ is the cross section, E is the relative collision energy, E_0 is the reaction threshold at 0 K, σ_0 is an energy-independent scaling factor, and n is an adjustable parameter that describes the energy deposition during collision. The summation is over the rovibrational states of the reactant ion having energies E_i with populations g_i, such that $\Sigma g_i = 1$. The integration is over the energy deposited into the ion by the collision, ϵ, and the exponential factor represents the probability of dissociation within the time window of the experiment. Here, τ is the average experimental time available for dissociation, and $k(\epsilon + E_i)$ is the unimolecular dissociation rate constant, calculated using RRKM theory.[17] Indices j refer to a particular product channel, and $k_{tot} = \Sigma k_j$. The ratio of dissociation rates, k_j/k_{tot}, introduces the coupling between product channels j. The scaling factors, $\sigma_{0,j}$, are ideally the same for all product channels, although previous experience[13] shows that separate scaling is sometimes

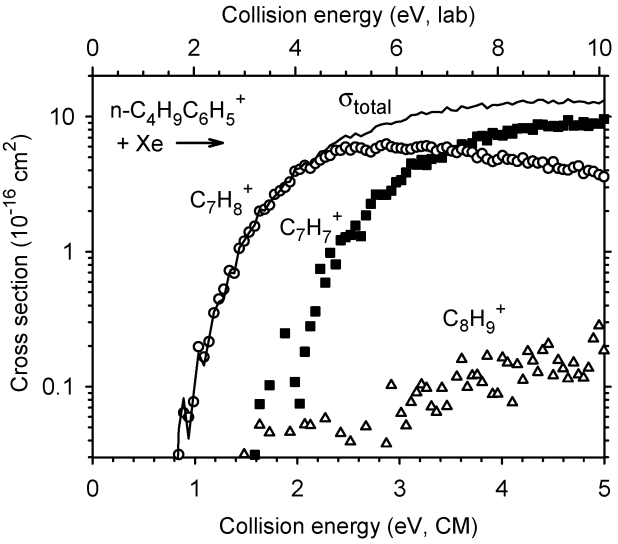

Figure 1. Integral cross sections as a function of energy for the CID of *n*-butylbenzene cation with Xe at a pressure of 0.1 mTorr. The products are $C_7H_8^+$ (circles), $C_7H_7^+$ (squares), and $C_8H_9^+$ (triangles).

needed to model data well or more detailed consideration of internal rotors is required.[37] The expression in eq 3 is further convoluted over the kinetic energy distributions of the two reactants before comparison with the data.[35] When individual modeling of the reaction channels is performed (competition not taken into account), we use an equation similar to eq 3 except that $k_{tot} = k_j$ of the channel of interest. When the kinetic shifts are ignored, we take the limit of an infinite experimental time τ in eq 3. In this latter case, the model collapses to the more familiar modified line-of-centers function.[38,39]

Results

Integral Cross Sections. Product cross sections for dissociation of *n*-$C_4H_9C_6H_5^+$ colliding with Xe as a function of energy were measured over the energy range from 0 to 5 eV in the center-of-mass frame and are presented in Figure 1. The first product observed is the $C_7H_8^+$ ion at 92 amu, with an apparent threshold around 0.8 eV, corresponding to reaction 2. The cross section of this product starts to decline concomitantly with the appearance of the second product, the $C_7H_7^+$ ion at 91 amu. This product is formed in reaction 1 and has an apparent threshold around 1.5 eV. The product cross sections have been corrected for mass overlap, which results from the 1 unit mass difference between the two products. Data were collected using a low-resolution setting on our quadrupole mass analyzer because this provides more efficient product collection over an extended energy range. At higher energies, we observe another product at 105 amu, presumably $C_8H_9^+$ corresponding to C_2H_5 loss. This cross section has an apparent threshold of about 2 eV and a small maximum cross section (less than ~0.3 Å^2). Because the contribution of this product to the total cross section is minor and does not interfere with the analysis of the first two products of reactions 1 and 2, we do not pursue analysis of this product channel further.

Calculation Results. To elucidate the details of the potential energy surface of this dissociation, a series of ab initio calculations was performed on the *n*-butylbenzene system using the Gaussian 98 suite of programs.[40] All optimized geometries and calculated frequencies for the reactant ion, products, and intermediates of interest were initially determined at the B3LYP/6-31G* level. Single-point energy calculations for structures of interest were performed at the B3LYP/6-311++G(2d,2p) level.

TABLE 2: Energy Calculations for *n*-Butylbenzene Ion Dissociation[a]

species	energy[b] (hartree)	ZPE[c] (hartree)	E_{rel}[d] (eV)
n-$C_6H_5C_4H_9^+$ [e]	−389.318 308	0.208 775	0
$C_7H_7^+$	−270.736 070	0.115 312	1.675
C_3H_7	−118.514 441	0.087 207	
$C_7H_8^+$	−271.321 606	0.124 621	1.081
C_3H_6	−117.951 324	0.078 509	
$TS_{0,60}$	−389.312 670	0.208 725	0.152
$Int_{0,120}$	−389.316 839	0.209 331	0.055
$TS_{60,120}$	−389.312 073	0.208 562	0.164
$Int_{120,120}$	−389.312 352	0.208 870	0.162
TS_{PT}	−389.284 140	0.205 305	0.835
Int_{PT}	−389.285 739	0.206 529	0.825
TS_{92}	−389.276 352	0.205 203	1.044
$[C_7H_8^+ \cdot C_3H_6]$	−389.279 483	0.203 573	0.915

[a] Different calculated transition states (TS) and intermediates (Int) are plotted in Figure 3 and described in the text. [b] Energies calculated at the B3LYP/6-311++G(2d,2p)//B3LYP/6-31G* level. [c] Zero-point energies (ZPE) calculated at the B3LYP/6-31G* level and scaled by 0.9804. [d] Relative energies, including zero-point energies. [e] Structure in Figure 2, nBB^+ in Figure 3, and assumed to be the global minimum.

For convenience, these results are referred to as B3LYP//B3LYP and are presented in Table 2. Single-point energy calculations were also performed at the MP2/6-311++G(2d,2p) level, but the values obtained for several points along the 92 amu dissociation channel were in severe disagreement with the experimental observations and with the other calculations. Therefore, we decided to exclude them from the present discussion. Vibrational frequencies and rotational constants were calculated for the relevant species and are presented in Table 3. The frequencies used in modeling were scaled by a factor of 0.9804,[41] unless otherwise noted. All intermediates and transition states discussed below were characterized as stationary points with either none or one imaginary frequency by detailed frequency calculations.

The most stable structure calculated for the *n*-butylbenzene cation, nBB^+, is presented in Figure 2. The structure has C_s symmetry, with the planes of the phenyl ring and the butyl chain oriented at 90° with respect to each other. This structure is consistent with previous computational studies on the *n*-butylbenzene neutral,[42,43] radical,[44,45] and cation,[43] along with spectroscopic investigations,[42,46] which all assume a similar structure as the most stable conformer. An alternate stable structure in which the butyl chain lies in the same plane as the phenyl ring was also identified but lies higher in energy by about 8.9 kJ/mol (B3LYP//B3LYP).

A series of reaction path calculations was performed to elucidate the dissociation mechanism. The 92 amu dissociation path, reaction 2, is investigated first, and in the following description, we use the C atom labels from Figure 2. The overall calculated potential energy surface for this dissociation is presented in Figure 3, where the calculated intermediate structures are shown. Geometrical details of these intermediate structures are available from the authors, by request. The investigations start at the geometry of the ground-state cation, nBB^+ (Figure 2), and they proceed through stepwise rotations of the butyl chain (at which point geometry optimizations and frequency calculations were performed) with the idea of reaching a geometry that enables proton transfer from the butyl chain to the ring. An initial rotation by 60° around the C_2-C_3 bond leads to a transition state, $TS_{0,60}$, situated at 0.152 eV, whereas another 60° rotation leads to a stable intermediate, $Int_{0,120}$, 0.055 eV higher than nBB^+. Next, a 60° rotation around the C_1-C_2 bond leads to a transition state, $TS_{60,120}$, situated at 0.164 eV, and

TABLE 3: Frequencies and Rotational Constants Used in Modeling CID and Rate Constant Data for *n*-Butylbenzene Ion Dissociation[a]

species	frequencies[b] (cm^{-1})	rot const (cm^{-1}) 1D	2D
n-$C_4H_9C_6H_5^+$ [c]	40, 64, 69, 119, 179, 234, 244, 343, 361, 364, 435, 527, 541, 627, 732, 767, 777, 789, 805, 847, 879, 928, 948, 976, 986, 986, 995, 1004, 1051, 1053, 1092, 1160, 1196, 1202, 1226, 1236, 1252, 1280, 1285, 1328, 1336, 1382, 1395, 1397, 1459, 1476, 1484, 1487, 1497, 1505, 1517, 1639, 2993, 2995, 3010, 3022, 3031, 3058, 3061, 3072, 3082, 3155, 3156, 3162, 3173, 3177	0.116	0.019
$C_7H_7^+$	3209, 3178, 3176, 3158, 3156, 3152, 3115, 1644, 1578, 1555, 1485, 1458, 1404, 1370, 1336, 1197, 1187, 1120, 1085, 1032, 1007, 995, 984, 984, 972, 835, 808, 785, 632, 617, 599, 524, 411, 352, 336, 162	0.178	0.075
n-C_3H_7	3193, 3098, 3059, 3051, 3001, 2984, 2966, 1506, 1495, 1485, 1462, 1398, 1320, 1300, 1186, 1083, 1014, 884, 738, 512, 328, 247, 77	1.044	0.278
$C_7H_8^+$	3214, 3173, 3163, 3153, 3150, 3119, 2950, 2937, 1577, 1554, 1517, 1495, 1429, 1404, 1366, 1328, 1299, 1189, 1175, 1173, 1050, 1019, 994, 974, 966, 966, 914, 900, 823, 769, 715, 580, 574, 491, 464, 409, 353, 243, 116	0.173	0.072
C_3H_6	3170, 3094, 3083, 3055, 3019, 2973, 1704, 1493, 1480, 1444, 1406, 1311, 1179, 1060, 1015, 936, 918, 913, 577, 415, 206	1.562	0.289
TS_{92}[d]	39, 67, 81, 125, 157, 178, 257, 310, 377, 442, 477, 520, 549, 619, 746, 756, 810, 853, 895, 956, 960, 970, 986,1006, 1030, 1040, 1047, 1059, 1064, 1086, 1110, 1124, 1243, 1252, 1253, 1267, 1351, 1362, 1411, 1465, 1471, 1481, 1504, 1509, 1548, 1562, 1573, 1601, 1614, 1663, 1710, 3076, 3129, 3151, 3196, 3264, 3284, 3293, 3301, 3328, 3338, 3347, 3359, 3382, 3395	0.089	0.021
TS_{91}[e]	11, 37, 46, 85, 99, 213, 230, 336, 337, 357, 377, 450, 528, 610, 634, 658, 773, 782, 824, 834, 841, 898, 901, 948, 957, 982, 984, 991, 995, 1024, 1026, 1114, 1127, 1193, 1198, 1203, 1288, 1303, 1349, 1351, 1390, 1407, 1475, 1484, 1500, 1500, 1505, 1525, 1558, 1577, 1629, 3031, 3041, 3081, 3120, 3129, 3136, 3156, 3179, 3180, 3186, 3200, 3204, 3237, 3252	0.104	0.014
n-$C_6H_5C_4H_9^+$ [f]	3000 (14), 1460 (11), 1260 (7), 1060 (10), 910 (6), 730 (5), 590 (2), 435 (4), 265 (4), 180 (1), 90 (2)		
TS_{92}[f]	3000 (14), 1460 (11), 1260 (7), 1060 (10), 910 (5), 730 (5), 600 (2), 500 (4), 400 (4), 300 (1), 250 (2)		
TS_{91}[f]	3000 (14), 1460 (11), 1260 (7), 1060 (10), 910 (5), 730 (5), 590 (2), 330 (4), 220 (4), 140 (1), 70 (2)		

[a] Calculated at the B3LYP/6-31G* level and scaled by a factor of 0.9804, unless otherwise noted. [b] Degeneracies in parentheses. [c] Structure in Figure 2, nBB^+, assumed to be the global minimum. [d] Calculated transition state for the 92 amu channel with frequencies scaled by an empirical factor of 1.039, which allows for the best RRKM reproduction of the experimental rates for this channel. [e] Calculated transient structure corresponding to $C_7H_7^+-C_3H_7$ at a C−C separation distance of 3.0 Å, assumed to be the transition state for the 91 amu channel. Frequencies are scaled by an empirical factor of 0.99, which allows for the best RRKM reproduction of the experimental rates for this channel. [f] Values assumed in the rate calculations of Baer et al., ref 27.

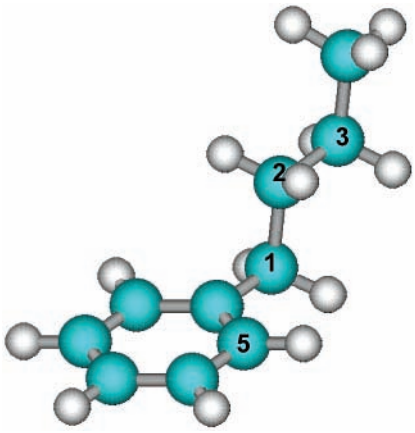

Figure 2. *n*-Butylbenzene cation, most stable structure, optimized at the B3LYP/6-31G* level of theory.

another 60° rotation reaches another stable intermediate, $Int_{120,120}$, only slightly lower in energy, 0.162 eV above nBB^+. This latter structure is in the proper orientation to promote a proton transfer from the C_3 atom of the butyl chain to the C_5 atom of the ring. Decreasing the distance between this H atom and the C_5 atom leads to a large increase in potential energy as the proton-transfer transition state, TS_{PT} at 0.835 eV, is formed. The nascent propene moiety moves further from the ring into a slightly lower in energy but stable intermediate, Int_{PT} at 0.825 eV. As the C_1-C_2 distance increases, another increase in the potential energy occurs, leading to the transition state TS_{92} situated 1.044 eV above the ground-state *n*-butylbenzene cation. This transition state corresponds to a distance of 2.1 Å between the separated C_1 and C_2 atoms of the chain. When the C_1-C_2 distance is further increased, the propene moiety shifts toward the stable product complex, PC, at 0.915 eV. The products lie in planes that are almost parallel to one another (a dihedral angle of 170.1°) at a distance of about 3.5 Å between the C_1 and C_2 atoms. An out-of-plane hydrogen from the C_5 atom of the ring is pointing toward the C_2-C_3 double bond of propene, consistent with a proton-bound π-complex. At large separations, the asymptotic product energy is calculated to be 1.081 eV, compared to the experimental value of 1.19 ± 0.14 eV (Table 1). Clearly, the most probable candidate for the rate-determining transition state for this dissociation is TS_{92}, not only because it is the highest in energy but also because of its structure, with the propene moiety just detached from the rest of the molecule.

The reaction path leading to propyl elimination, reaction 1, is also investigated. Starting at the *n*-butylbenzene ion geometry, the distance between the C_1 and C_2 atoms is systematically increased while allowing the unrestricted optimization of all other coordinates. A direct dissociation curve is obtained, as presented in Figure 4. The curve is compared to the ion−induced dipole model prediction, which is usually employed to approximate the long-range interaction between ionic and neutral products. This ion−induced dipole potential is expressed as

$$V(r) = -\alpha q^2/8\pi\epsilon_0 r^4 \qquad (4)$$

where α is the polarizability volume of the neutral product (for C_3H_7, we used the value for propane,[47] 6.29 $Å^3$), q is the charge of the ionic product, ϵ_0 is the permittivity of vacuum, and r is the distance between the separating products. The model in Figure 4 is calculated using the separation distance between the C_1 and C_2 atoms of the two products, for consistency with the calculation. Clearly, the calculated energy has a different radial dependence, but there is good agreement with the ion−

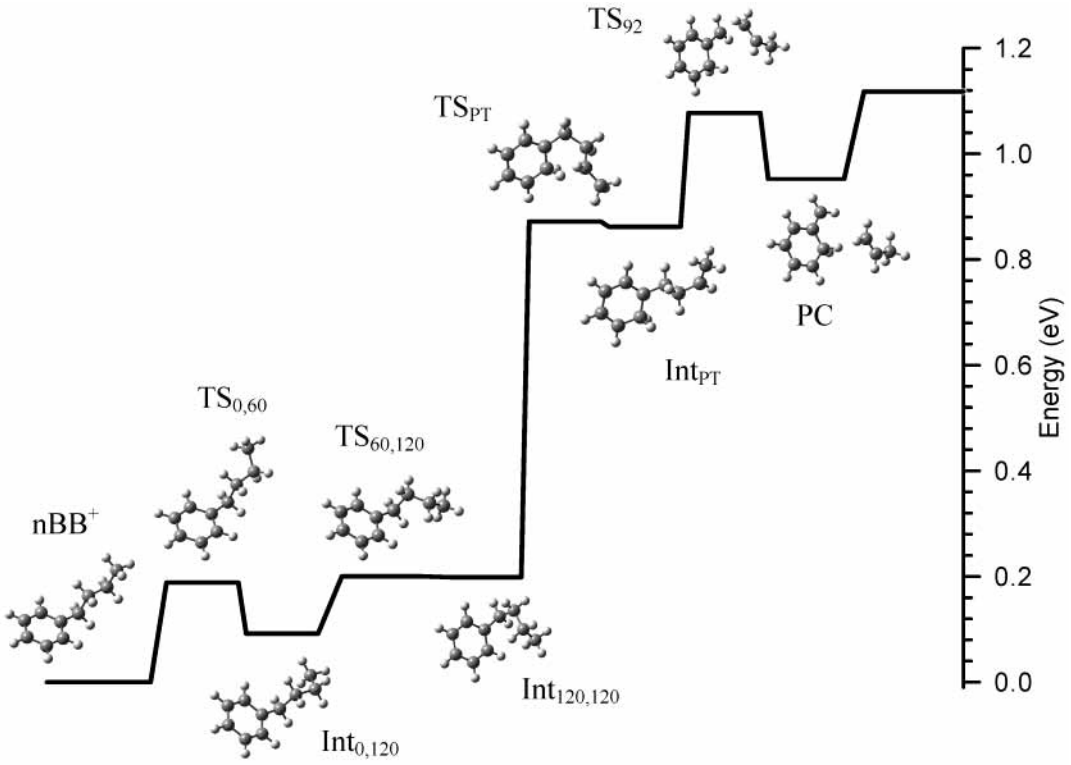

Figure 3. Calculated potential energy curve for the 92 amu *n*-butylbenzene cation dissociation by loss of propene at the B3LYP/6-311++G(2d,-2p)//B3LYP/6-31G* level. The origin represents nBB^+, the ground-state *n*-butylbenzene cation (Figure 2). The different structures are optimized at the B3LYP/6-31G* level, and their notations are described in the text.

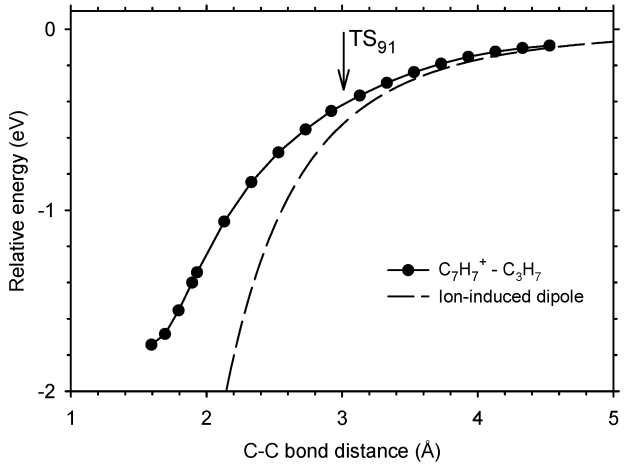

Figure 4. Dissociation path energy calculations for $C_7H_7^+-C_3H_7$ (circles) as a function of the separating C−C distance, performed at the B3LYP/6-31G* level of theory. The dashed line indicates the prediction of the ion−induced dipole interaction potential, eq 4, as a function of the same C−C distance with parameters indicated in text. The position at which we calculate the structure used as the optimal transition state for the 91 amu channel is indicated by the arrow.

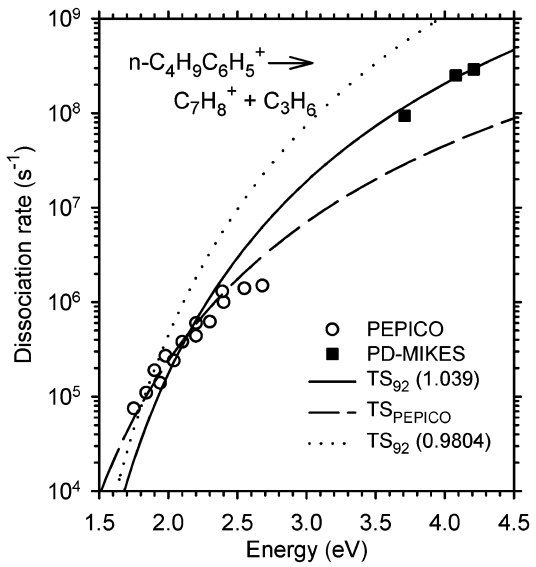

Figure 5. RRKM modeling of unimolecular dissociation rates for the 92 amu channel (propene elimination) of the *n*-butylbenzene cation as a function of energy. Experimental points represent PEPICO measurements (open circles, ref 27) and PD-MIKES measurements (closed squares, ref 28). The energy scale represents the internal energy of the *n*-butylbenzene cations. The lines represent RRKM rates calculated using the rate-determining transition state, TS_{92}, with frequencies scaled by an empirical factor of 1.039 and a 0 K threshold of 1.15 eV (solid line); the transition state assumed by Baer et al.[27] for a threshold of 0.97 eV (dashed line); and TS_{92} with frequencies scaled by the recommended factor of 0.9804 and a 0 K threshold of 1.15 eV (dotted line).

induced dipole potential for the long-range interactions, beyond about 3.5 Å.

Dissociation Rate Modeling. The unimolecular dissociation rates of the system with respect to reactions 1 and 2 as a function of energy are calculated here using RRKM theory. We consider several different assumptions about the most probable transition states, as described below. For each TS assumed, the value of the activation energy (the 0 K dissociation threshold) is varied until the best agreement is achieved with the experimental unimolecular dissociation rates obtained in the PEPICO[27] and PD-MIKES[28] experiments. In these studies, experimental rates are measured only for the 92 amu product, reaction 2, as presented in Figure 5. Both studies derive experimental values for the 91 amu product rates (Figure 6) from the measured 91/92 branching ratios and from a good fit of the 92 amu rate. The RRKM fits are evaluated using the vibrational frequencies and

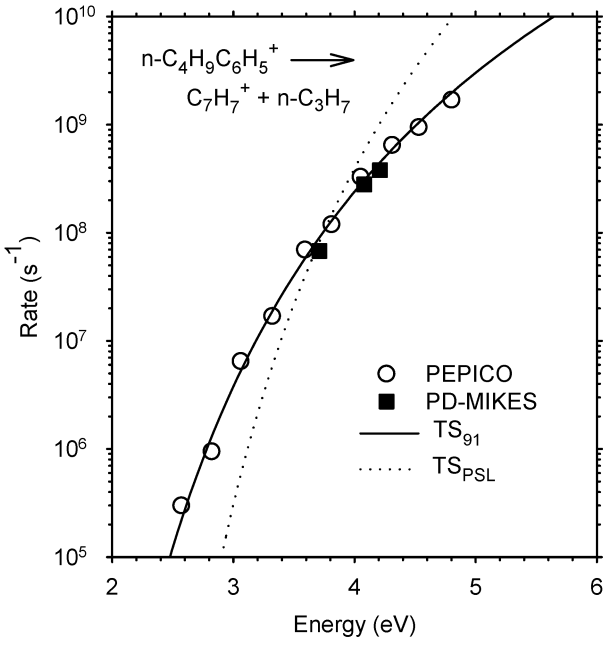

Figure 6. RRKM modeling of unimolecular dissociation rates for the 91 amu channel (propyl elimination) of the *n*-butylbenzene cation as a function of energy. Experimental points represent PEPICO measurements (open circles, ref 27) and PD-MIKES measurements (closed squares, ref 28). The energy scale represents the internal energy of the *n*-butylbenzene cations. The lines represent RRKM rates calculated using TS_{91}, the calculated transition state located at 3.0 Å separation between the two products, with frequencies scaled by an empirical factor of 0.99 and a 0 K threshold of 1.57 eV (solid line) and the PSL model transition state for a threshold of 2.3 eV (dotted line).

rotational constants calculated at the B3LYP/6-31G* level, with vibrations scaled by 0.9804, as reported in Table 3. A reaction degeneracy of 1 for each channel is assumed for all of the calculations. When we used a reaction degeneracy of $^1/_2$ for the 91 amu channel, as derived from the symmetry number of 2 for benzyl cation, the difference in the thresholds obtained was negligible (0.005 eV) compared to the other uncertainties. For the PEPICO data, we take the initial internal energy of the reactants into account by simply shifting the energy scale of the rate constants by the average internal energy of *n*-butylbenzene cations at the temperature of their experiment (300 K). More exactly, the energy scale for the PEPICO data represents $E_{h\nu} - \mathrm{IE} + E_{\mathrm{th}}$, where $E_{h\nu}$ is the photon energy; IE is the ionization energy of *n*-butylbenzene (8.69 ± 0.01 eV, Table 1); and E_{th} is the average thermal energy of *n*-butylbenzene at 300 K (0.25 eV), calculated using the vibrational frequencies in Table 3. For the PD-MIKES data, the authors follow a similar procedure, except that they estimated the distribution of undissociated ions that reach the laser interaction region and used this average to shift the energy scale. For the PEPICO data, we tried to apply the more complicated, correct procedure of convoluting the calculated rates over the internal energy distribution of the *n*-butylbenzene cations at the proper temperature (300 K), but no significant difference was observed. This is mainly because the energy range of the rate data is significantly higher than the dissociation thresholds. The uncertainties reported for the dissociation energies derived from fitting the unimolecular dissociation rates are as reported in the original PEPICO experiments, ±0.1 eV.

For the 92 amu channel, reaction 2, we first considered the calculated transition state, TS_{92} in Figure 3, which connects the molecular ion to the $C_7H_8^+ - C_3H_6$ product complex using frequencies scaled by 0.9804. The slope of the calculated rate was too large, indicating that this transition state is too loose. To make it tighter, we scaled all of its vibrational frequencies up by different factors, until the slope of the calculated rate was compatible with the rate data. A transition state TS_{92} whose frequencies are scaled by 1.039 was used for the rate calculated and presented in Figure 5, which reproduces the experimental rates with the best accuracy. The 0 K threshold energy corresponding to this calculated rate is 1.15 eV, and the activation entropy at 1000 K is $\Delta S^{\ddagger} = -19.1$ J/K mol, indicating a fairly tight transition state. We also tried to reproduce the rate data of Baer et al.[27] using the same RRKM procedure as for the calculations described above but with the transition state parameters (TS_{PEPICO}) used by these authors (Table 3). In their calculation, because of the lack of available calculated frequencies, the authors combined known frequencies of smaller neutral molecules into a set of reasonable frequencies for the molecular ion. For the transition state (Table 3), they scaled down some of these frequencies to different arbitrary extents until the best reproduction of experimental rates was achieved. The best fit (Figure 5) was obtained for a threshold value of 0.97 eV, in good agreement with the value of 0.99 ± 0.10 eV reported by Baer et al. We also obtained an activation entropy of $\Delta S^{\ddagger} = -45.9$ J/K mol, similar to the value reported by Baer et al., $\Delta S^{\ddagger} = -45.6$ J/K mol, values that indicate a significantly tight transition state. We note that these calculated rates reproduce the PEPICO data very well but are ∼5 times smaller than the PD-MIKES values measured by Oh et al.,[28] which were unavailable to Baer et al. This difference is an indication that the transition state parameters assumed by Baer et al. are inexact. Oh et al.[28] also performed RRKM modeling of their data along with the PEPICO data and obtained a threshold value of 1.12 eV and an activation entropy of $\Delta S^{\ddagger} = -23.0$ J/K mol. They used the same vibrational frequencies for the parent molecule as Baer et al. and a similar procedure of arbitrarily adjusting the vibrational frequencies of the transition state until a good fit to the rates was obtained. The fact that these values are comparable to ours indicates that the detailed values of the molecular constants are not critical to reproducing the data or the final modeling parameters, E_0 and $\Delta S^{\ddagger}$.

The 91 amu rate points presented in Figure 6 are derived from the PEPICO and PD-MIKES experimental branching ratios and from our best fit to the 92 amu rate data, labeled "TS_{92}" in Figure 5. For this channel, reaction 1, we started by assuming a loose transition state in the phase-space limit[12] (PSL), with parameters corresponding to the two separated products. This is usually the choice for an ion−induced dipole interaction between the products. Further, the potential energy surface for the propyl elimination described in the previous section (Figure 4) indicates that the ion−induced dipole model might be reasonable for the long-range interactions. The RRKM rates calculated using the PSL transition state assumption are presented in Figure 6. Their slope is much higher than that of the data, indicating that the PSL assumption is not the proper choice for this system. This is consistent with our previous conclusions for covalent bond cleavages, as elucidated in our study on dichlorobenzene cation dissociation.[15]

In analogy with that study, a different approach was followed next. Transient structures were calculated along the dissociation path (Figure 4) for several separation distances between the C_1 and C_2 atoms of the two separating products: 2.19, 2.59, 2.80, 3.00, 3.20, 3.50, and 4.00 Å. Each of the transient structures was assumed as a transition state and used in an RRKM calculation of the dissociation rates. The calculated rates were

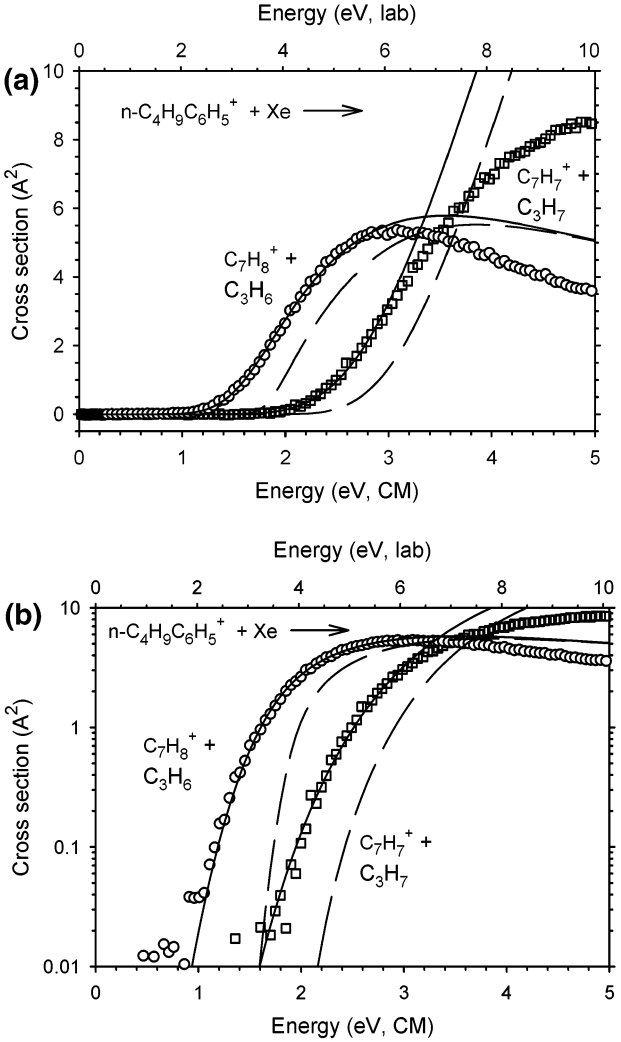

Figure 7. Modeling of the CID cross sections for *n*-butylbenzene cation dissociation using eq 3 with the parameters indicated in Table 4 and using the set of transition states, TS_{91} and TS_{92} (Table 3), that reproduce the experimental dissociation rates. The symbols represent the cross-section data extrapolated to zero Xe pressure, the dashed line represents the model for reactants with an internal temperature of 0 K, and the solid line represents the same model convoluted over the kinetic and internal energy distributions of the two reactants. Parts a and b show the same material on linear and logarithmic scales, respectively.

then compared to the experimental ones, and a decision was made about the appropriateness of the particular transition state. Following this approach, the best reproduction (Figure 6) of the experimental rates was obtained with a transition state, TS_{91}, located at 3.0 Å separation between C_1 and C_2 of the two products, after minor scaling of the vibrational frequencies (a factor of 0.99). The 0 K threshold energy used in this RRKM calculation was 1.57 eV, and the activation entropy was $\Delta S^{\ddagger} = 32.6$ J/K mol, which indicates a loose transition state. The molecular constants of this transition state, TS_{91}, are presented in Table 3.

CID Cross Section Modeling. CID cross sections are modeled using the procedure described in the data analysis section. The model of eq 3 includes RRKM theory to account for kinetic shifts and competition between the two product channels. A representative model fit to the CID data is presented in Figure 7. Uncertainties in the threshold energies were calculated considering several sources: the variation of optimized fit parameters among different data files, the range of parameters that allow reasonably good reproduction of one data set, the range of threshold energies that yield good fits of rate constant data, and the uncertainty in the collision energy calibration (± 0.025 eV, CM frame). The final results are presented in Table 4.

We first consider the transition state combination, TS_{91}, TS_{92}, that led to the best RRKM reproduction of the dissociation rate data. The CID fits are presented in Figure 7, and we observe that they reproduce the CID cross-section data for more than 2 orders of magnitude in cross section and up to about 3 eV in energy, including the curvature of the 92 amu channel resulting from competition. The 0 K threshold values of these fits are 1.28 ± 0.06 eV for the 92 amu channel and 1.70 ± 0.09 eV for the 91 amu channel. The other parameters of the fits are presented in Table 4. These model parameters were chosen to reproduce the threshold region of the cross sections with high fidelity. Using different parameters, the model can also reproduce the higher-energy part of the data, but at the expense of a poor fit in the threshold region, which we consider unacceptable.

Next, it is interesting to determine the kinetic and competitive shifts of the system, the effect of excluding competition and RRKM calculations from our modeling procedure. When we perform individual modeling of the dissociation channels (no competition included), we obtain thresholds of 1.22 ± 0.09 and 1.87 ± 0.10 eV for the 92 and 91 amu channels, respectively (Table 4). The competitive shift is significant for the higher-energy channel, a difference of 0.17 eV for the 91 amu threshold, outside the uncertainties of our determinations. When we exclude both the RRKM analysis and the competition from our modeling, the thresholds obtained are 1.62 ± 0.09 and 2.61 ± 0.10 eV, respectively (Table 4). These values indicate significant kinetic shifts: about 0.40 and 0.74 eV for the 92 and 91 amu channels, respectively.

Finally, it would be interesting to explore the threshold values that would have been obtained if we had not had a set of experimental dissociation rates to adjust and scale the calculated transition states. In that case, for the 92 amu channel, we would have used the parameters of the calculated transition state, scaled by the recommended factor of 0.9804. For the 91 amu channel, the first choice would have been the PSL assumption for the transition state. With these assumptions, cross-section modeling gives 0 K thresholds of 1.25 ± 0.06 and 1.96 ± 0.09 eV and activation entropies of 3.1 and 90.0 J/K mol for the 92 and 91 amu channels, respectively (Table 4). If, instead of the PSL assumption, we had considered a transient structure situated at 3.5 Å separation between products (Figure 4), where the potential energy of the system approaches that of the ion−induced dipole model, the thresholds would have been 1.29 ± 0.06 and 1.72 ± 0.09 eV and the activation entropies 3.1 and 51.7 J/K mol for the 92 and 91 amu channels, respectively (Table 4). These results are very similar to those obtained via our competitive analysis using the best transition state parameters.

Discussion

The process of assessing correct CID thresholds for systems affected by kinetic and competitive shifts is not straightforward. Our model, eq 3, that accounts for these shifts requires critical input in terms of the transition state parameters of a particular dissociation. A complicating factor is that the part of the cross section whose shape is most affected by these shifts (the lowest energies) can be obscured in the noise, which reduces the ability of our model to discriminate between the several possible transition states, as also observed before.[15,16] Therefore, to make a proper choice of a transition state, we cannot rely on CID

TABLE 4: 0 K Threshold Values for *n*-Butylbenzene Ion Dissociation

	E_0 (eV)		$\Delta S^{\ddagger}_{1000}$ [J/(K mol)]		σ_0		n	
source	91	92	91	92	91	92	91	92
CID competition[a]	1.70 (0.09)	1.28 (0.06)	32.6	−19.1	76 (30)	14 (5)	0.96 (0.15)	
CID individual[b]	1.87 (0.10)	1.22 (0.09)			18 (4)	11 (4)	1.07 (0.20)	1.37 (0.40)
CID no RRKM[c]	2.61 (0.10)	1.62 (0.09)			16 (4)	10 (3)	1.16 (0.20)	1.49 (0.40)
CID PSL/TS_{92}[d]	1.96 (0.09)	1.25 (0.06)	89.7	3.1	21 (10)	13 (5)	1.36 (0.15)	
CID 3.5 Å/TS_{92}[e]	1.72 (0.09)	1.29 (0.06)	51.7	3.1	63 (28)	13 (5)	1.07 (0.15)	
rates[f]	1.57 (0.10)	1.15 (0.10)	32.6	−19.1				
rates (Baer)[g]	1.61 (0.10)	0.99 (0.10)	14.6	−45.9				
rates (Oh)[h]	1.61	1.12	30.5	−23.0				
calculations[i]	1.68	1.08						
literature[j]	1.80 (0.05)	1.19 (0.14)						

[a] CID modeling using eq 3 with the optimal transition states, TS_{91} and TS_{92}, the ones that allow the best reproduction of dissociation rate data (Table 3). [b] CID modeling of individual channels using the optimal transition states. [c] CID modeling of individual channels, without RRKM analysis. [d] CID modeling using eq 3 with the calculated transition state for the 92 amu channel and with the PSL loose transition state assumed for the 91 amu channel, both scaled by the recommended factor of 0.9804. [e] CID modeling using eq 3 with the calculated transition state for the 92 amu channel and with the calculated transient structure at 3.5 Å product separation for the 91 amu channel, both scaled by the recommended factor of 0.9804. [f] RRKM modeling of dissociation rates from PEPICO and PD-MIKES experiments using the optimal transition states calculated in this work. [g] RRKM modeling of PEPICO dissociation rates from ref 27. [h] RRKM modeling of PEPICO and PD-MIKES dissociation rates from ref 28. [i] Ab initio calculations using B3LYP/6-311++G(2d,2p)//B3LYP/6-31G* for the product asymptote of the 91 and 92 amu channels. [j] Literature values for the product asymptotes, from Table 1.

data reproduction alone, and we usually employ the knowledge provided by theoretical calculations to make an appropriate choice. In this particular case, a carefully selected test study, we also have unimolecular dissociation rate data to guide us on the proper choice of a transition state. Here, we use this additional information to educate ourselves about the best choice of a transition state for other compatible systems considered in the future.

Although the *n*-butylbenzene cation dissociation has been studied experimentally often for its application as a molecular "thermometer", there has been no theoretical investigation of its dissociation mechanism until now. The propyl elimination reaction 1 has been intuitively assumed to be a simple bond-breaking dissociation,[22,27] and our reaction path calculation (Figure 4) confirms this possibility. In addition, we compare the potential energy calculated for the interaction between the two products with the prediction of the ion−induced dipole model. The comparison indicates that the interaction can be reasonably described by the model in the long-range limit (>3.5 Å) if the distances are defined relative to the closest C atoms (C_1-C_2) and not with respect to the centers of mass of the two fragments. This definition of the separation distances is consistent with the observations of our previous study on the dissociation of the dichlorobenzene molecule[15] and is a consequence of the covalent interactions in these dissociations being shorter-range (stronger) than the ones assumed in the model.

In terms of transition state selection, the agreement of the calculated potential with the ion−induced dipole model indicates that a PSL loose transition state might be appropriate for the description of this dissociation, but the RRKM calculation using this transition state fails to fit the experimental dissociation rates (Figure 6). The rates are reproduced by a fixed transition state located at a distance of 3.0 Å, where the calculated potential energy and the ion−induced dipole model start to diverge from one another. This indicates that the PSL model fails to describe a direct bond cleavage for a C−C bond. A similar observation was made in our previous study for cleavage of a C−Cl bond: the dissociation of the dichlorobenzene cation.[15] This observation is not surprising if we consider that the PSL model was devised for weak electrostatic interactions and we encounter here a covalent chemical bond. In this case, the availability of dissociation rate data was essential in determining the correct transition state, in addition to the calculations. Nevertheless, if we did not have the rate data and we assumed a transition state located where the calculated potential energy (Figure 4) approached the ion−induced dipole model, at 3.5 Å, the CID threshold obtained would be 1.72 ± 0.09 eV (Table 4). This is very close, well within uncertainties, to the value obtained with the correct transition state, 1.70 ± 0.09 eV. This appears to be the best upper-limit approximation to follow when one lacks the feedback from experimental dissociation rates for a system that dissociates by breaking a fairly strong chemical bond. By contrast, if we assumed a PSL loose transition state, the CID threshold would shift up to 1.96 ± 0.09 eV, which is clearly an upper limit to the value obtained with the best transition state.

The mechanism of the other dissociation channel, the propene elimination reaction 2, is less straightforward. A proton transfer process followed by an isomerization reaction (McLafferty rearrangement) was previously postulated,[27,28] and our calculations provide detailed insight into this pathway. The reaction path calculations indicate that the propene elimination proceeds as follows: First, a rotation of the alkyl chain toward the ring occurs, which allows for H atom transfer from C_3 to the C_5 atom in the ring (Int_{PT}, Figure 3). Then, a slight separation of atoms C_1 and C_2 of the chain leads to the transition state (TS_{92}, Figure 3). Further, the detached propene translates toward a proton-bound π-complex with the methylene−cyclohexadiene (PC, Figure 3). Finally, the complex dissociates directly into the two products. The RRKM calculation using the transition state found on this path reproduces the experimental dissociation rates reasonably well (Figure 5), a good indication that we found the rate-limiting transition state for this channel. The comparison with the experimental rates helps us to find the best scaling factors of the calculated vibrational frequencies for the transition state (1.039) and also to identify the range of uncertainties associated with this factor. If we did not have the experimental dissociation rates and we used the calculated transition state only scaled by the recommended factor of 0.9804, we would obtain the CID thresholds indicated in Table 4. The values, 1.29 ± 0.06 or 1.25 ± 0.06 eV (depending on the transition state selection for the 91 amu channel), are within the uncertainties of the threshold obtained when the optimally scaled transition state is used, 1.28 ± 0.06 eV. This indicates that, in the case of dissociation through molecular rearrangement, a good approximation is to use the rate-determining, calculated transition state.

We can now compare our CID threshold values with the values obtained from modeling the experimental dissociation rates, with reported values from the literature, and with the calculated thresholds (Table 4). The values determined through CID (1.70 ± 0.09 and 1.28 ± 0.06 eV) and rate constant modeling (1.57 ± 0.10 and 1.15 ± 0.10 eV) are within their combined uncertainties, although the CID values are higher by 0.13 eV for both channels. For the 91 amu channel, the CID value of 1.70 ± 0.09 eV is in better agreement with the literature value of 1.80 ± 0.05 eV, determined from the known heats of formation of the parent and product molecules (Table 1). For the 92 amu channel, the literature value, 1.19 ± 0.14 eV, has large uncertainties, especially because of the poorly known heat of formation of the methylene-1,3-cyclohexadiene ion. Within these uncertainties, both the CID value, 1.28 ± 0.06 eV, and the threshold from modeling the rate data, 1.15 ± 0.10 eV, are in agreement, but because of such large uncertainties, the comparison is less meaningful. The B3LYP energies reproduce the general trend of the different experimental values with good accuracy.

Conclusions

The threshold collision-induced dissociation of *n*-butylbenzene cations was investigated over an energy range from 0 to 5 eV in the center-of-mass frame. The competitive dissociations leading to propyl and propene elimination were investigated in detail.

Ab initio calculations were employed to investigate the dissociation mechanisms and to provide molecular parameters needed for the data modeling. Reaction path calculations indicate that the propyl elimination proceeds through a direct bond rupture. An ion−induced dipole model reproduces the interaction between the products at C−C distances larger than about 3.5 Å. For the 92 amu channel, reaction path calculations suggest that the propene elimination reaction proceeds through a chain rotation followed by hydrogen transfer and incipient C−C bond cleavage, to form a product complex that separates into the two products. A rate-limiting transition state was positively identified on this reaction path.

Unimolecular dissociation rates as a function of energy from PEPICO[27] and PD-MIKES[28] experiments were modeled using RRKM theory to find the proper transition state parameters for the two dissociation channels. For the 91 amu channel, the best transition state is a transient structure calculated at 3.0 Å separation between the two products, whose vibrational frequencies are scaled by an empirical factor of 0.99 (instead of the recommended 0.9804) and for a 0 K threshold of 1.57 ± 0.10 eV. For the 92 amu channel, the best transition state is the rate-determining, calculated transition state with vibrational frequencies scaled by an empirical factor of 1.039 (instead of the recommended 0.9804) and for a 0 K threshold of 1.15 ± 0.10 eV. CID cross sections were fit using a model that accounts for both kinetic and competitive shifts, using the best transition states determined through modeling of the experimental dissociation rates. The 0 K CID thresholds obtained are 1.70 ± 0.09 eV for the 91 amu channel and 1.28 ± 0.06 eV for the 92 amu channel. These values are in reasonable agreement with the known literature values, 1.80 ± 0.05 and 1.19 ± 0.14 eV, respectively, within the combined uncertainties.

On the basis of the current and previous[15,16] studies, we can identify procedures of selecting the transition states with good approximation for similar systems, when the feedback obtained from experimental dissociation rates is not available. For dissociation through simple bond rupture of a covalent chemical bond (e.g., the 91 amu channel), a reasonable transition state could be calculated as the transient structure situated at the minimal separation between the two products where the interaction energies start to be reproduced by a ion−induced dipole model. Distances between the heavy atoms of the bond to be broken should be used instead of distances between the centers of mass of the two products. For dissociation through molecular rearrangement (92 amu channel), the rate-determining transition state, identified through ab initio calculations, represents a reasonable choice.

Acknowledgment. This work is supported by the National Science Foundation, Grant No. CHE-0135717.

References and Notes

(1) Tiernan, T. O.; Wu, R. L. *Adv. Mass Spectrom.* **1978**, *7A*, 136.
(2) Squires, R. R. *Int. J. Mass Spectrom. Ion Processes* **1992**, *117*, 565.
(3) Magnera, T. F.; David, D. E.; Michl, J. *J. Am. Chem. Soc.* **1989**, *111*, 4100.
(4) Armentrout, P. B. *Acc. Chem. Res.* **1995**, *28*, 430.
(5) Klassen, J. S.; Anderson, S. G.; Blades, A. T.; Kebarle, P. *J. Phys. Chem.* **1996**, *100*, 14218.
(6) Grushow, A.; Ervin, K. M. *J. Am. Chem. Soc.* **1995**, *117*, 11612.
(7) Sowa-Resat, M. B.; Hintz, P. A.; Anderson, S. L. *J. Phys. Chem.* **1995**, *99*, 10736.
(8) Deng, H. T.; Kerns, K. P.; Castleman, A. W. *J. Phys. Chem.* **1996**, *100*, 13386.
(9) Amunugama, R.; Rodgers, M. T. *Int. J. Mass Spectrom.* **2000**, *195/196*, 439.
(10) Loh, S. K.; Hales, D. A.; Lian, L.; Armentrout, P. B. *J. Chem. Phys.* **1989**, *90*, 5466.
(11) Khan, F. A.; Clemmer, D. E.; Schultz, R. H.; Armentrout, P. B. *J. Phys. Chem.* **1993**, *97*, 7978.
(12) Rodgers, M. T.; Ervin, K. M.; Armentrout, P. B. *J. Chem. Phys.* **1997**, *106*, 4499.
(13) Rodgers, M. T.; Armentrout, P. B. *J. Chem. Phys.* **1998**, *109*, 1787.
(14) Muntean, F.; Armentrout, P. B. *J. Chem. Phys.* **2001**, *115*, 1213.
(15) Muntean, F.; Heumann, L.; Armentrout, P. B. *J. Chem. Phys.* **2002**, *116*, 5593.
(16) Muntean, F.; Armentrout, P. B. *J. Phys. Chem. B* **2002**, *106*, 8117.
(17) See for example Gilbert, R. G.; Smith, S. C. *Theory of Unimolecular and Recombination Reactions*; Blackwell Scientific Publications: Oxford, U.K., 1990.
(18) Mukhtar, E. S.; Griffith, I. W.; Harris, F. M.; Beynon, J. H. *Int. J. Mass Spectrom. Ion Phys.* **1981**, *37*, 159.
(19) Griffith, I. W.; Mukhtar, E. S.; March, R. E.; Harris, F. M.; Beynon, J. H. *Int. J. Mass Spectrom. Ion Phys.* **1981**, *39*, 125.
(20) Griffith, I. W.; Mukhtar, E. S.; Harris, F. M.; Beynon, J. H. *Int. J. Mass Spectrom. Ion Phys.* **1982**, *43*, 283.
(21) Welch, M. J.; Pereles, D. J.; White, E. *Org. Mass Spectrom.* **1985**, *20*, 425.
(22) Chen, J. H.; Hays, J. D.; Dunbar, R. C. *J. Phys. Chem.* **1984**, *88*, 4759.
(23) Nacson, S.; Harrison, A. G. *Int. J. Mass Spectrom. Ion Processes* **1985**, *63*, 85.
(24) Harrison, A. G.; Lin, M. S. *Int. J. Mass Spectrom. Ion Phys.* **1983**, *51*, 353.
(25) McLuckey, S. A.; Ouwerkerk, C. E. D.; Boerboom, A. J. H.; Kistemaker, P. J. *Int. J. Mass Spectrom. Ion Processes* **1984**, *59*, 85.
(26) McLuckey, S. A.; Sallans, L.; Cody, R. B.; Burnier, R. C.; Verma, S.; Freiser, B. S.; Cooks, R. G. *Int. J. Mass Spectrom. Ion Phys.* **1982**, *44*, 215.
(27) Baer, T.; Dutuit, O.; Mestdagh, H.; Rolando, C. *J. Phys. Chem.* **1988**, *92*, 5674.
(28) Oh, S. T.; Choe, J. C.; Kim, M. S. *J. Phys. Chem.* **1996**, *100*, 13367.
(29) Yoon, O. K.; Hwang, W. G.; Choe, J. C.; Kim, M. S. *Rapid Commun. Mass Spectrom.* **1999**, *13*, 1515.
(30) Burgers, P. C.; Terlouw, J. K.; Levsen, K. *Org. Mass Spectrom.* **1982**, *17*, 295.
(31) Holmes, J. L.; Osborne, A. D. *Org. Mass Spectrom.* **1981**, *16*, 236.
(32) Linstrom, P. J.; Mallard, W. G., Eds. *NIST Chemistry WebBook*; NIST Standard Reference Database Number 69; National Institute of Standards and Technology: Gaithersburg, MD, 2003 (http://webbook.nist.gov, accessed Mar 2003).
(33) Average of three values from: Marshall, R. M.; Rahman, L. *Int. J. Chem. Kinet.* **1977**, *9*, 705. Tsang, W. J. *J. Am. Chem. Soc.* **1985**, *107*, 2872. Holmes, J. L.; Lossing, F. P.; Maccoll, A. *J. Am. Chem. Soc.* **1988**, *110*, 7339.

(34) Pedley, J. B.; Naylor, R. D.; Kirby, S. P. *Thermochemical Data of Organic Compounds*, 2nd ed.; Chapman and Hall: London, 1986.
(35) Ervin, K. M.; Armentrout, P. B. *J. Chem. Phys.* **1985**, *83*, 166.
(36) Daly, N. R. *Rev. Sci. Instrum.* **1959**, *31*, 264.
(37) Amicangelo, J. C.; Armentrout, P. B. *Int. J. Mass Spectrom.* **2001**, *212*, 301.
(38) Schultz, R. H.; Crellin, K. C.; Armentrout, P. B. *J. Am. Chem. Soc.* **1991**, *113*, 8590.
(39) Levine, R. D.; Bernstein, R. B. *Molecular Reaction Dynamics and Chemical Reactivity*; Oxford University Press: New York, 1987.
(40) Frisch, M. J.; Trucks, G. W.; Schlegel, H. B.; Scuseria, G. E.; Robb, M. A.; Cheeseman, J. R.; Zakrzewski, V. G.; Montgomery, J. A., Jr.; Stratmann, R. E.; Burant, J. C.; Dapprich, S.; Millam, J. M.; Daniels, A. D.; Kudin, K. N.; Strain, M. C.; Farkas, O.; Tomasi, J.; Barone, V.; Cossi, M.; Cammi, R.; Mennucci, B.; Pomelli, C.; Adamo, C.; Clifford, S.; Ochterski, J.; Petersson, G. A.; Ayala, P. Y.; Cui, Q.; Morokuma, K.; Malick, D. K.; Rabuck, A. D.; Raghavachari, K.; Foresman, J. B.; Cioslowski, J.; Ortiz., Baboul, A. G.; J. V.; Stefanov, B. B.; Liu, G.; Liashenko, A.; Piskorz, P.; Komaromi, I.; Gomperts, R.; Martin, R. L.; Fox, D. J.; Keith, T.;; Al-Laham, M. A.; Peng, C. Y.; Nanayakkara, A.; Challacombe, M.; Gill, P. M. W.; Johnson, B.; Chen, W.; Wong, M. W.; Andres, J. L.; Gonzalez, C.; Head-Gordon, M.; Replogle, E. S.; Pople, J. A. *Gaussian 98*, Revision A.11; Gaussian, Inc.: Pittsburgh, PA, 1998.
(41) Foresman, J. B.; Frisch, A. E. *Exploring Chemistry with Electronic Structure Methods*, 2nd ed.; Gaussian, Inc.: Pittsburgh, PA, 1996.
(42) Dickinson, J. A.; Joireman, P. W.; Kroemer, R. T.; Robertson, E. G.; Simons, J. P. *J. Chem. Soc., Faraday Trans.* **1997**, *93*, 1467.
(43) Patey, M. D.; Dessent, C. E. H. *J. Phys. Chem. A* **2002**, *106*, 4623.
(44) van Speybroeck, V.; van Neck, D.; Waroquier, M.; Wauters, S.; Saeys, M.; Marin, G. B. *Int. J. Quantum Chem.* **2003**, *91*, 384.
(45) van Speybroeck, V.; Borremans, Y.; Van Neck, D.; Waroquier, M.; Wauters, S.; Saeys, M.; Marin, G. B. *J. Phys. Chem. A* **2001**, *105*, 7713.
(46) Mate, B.; Suenram, R. D.; Lugez, C. *J. Chem. Phys.* **2000**, *113*, 192.
(47) Miller, K. J. *J. Am. Chem. Soc.* **1990**, *112*, 8533.